Ultrafast Terahertz Photoconductivity of Photovoltaic Polymer–Fullerene Blends: A Comparative Study Correlated with Photovoltaic Device Performance

ARTICLE *in* JOURNAL OF PHYSICAL CHEMISTRY LETTERS · NOVEMBER 2014

Impact Factor: 7.46 · DOI: 10.1021/jz501890n

7 AUTHORS, INCLUDING:

Zuanming Jin
Max Planck Institute for Polymer Research
44 PUBLICATIONS **172** CITATIONS
SEE PROFILE

Frédéric Laquai
King Abdullah University of Science and Tec…
101 PUBLICATIONS **2,027** CITATIONS
SEE PROFILE

Mischa Bonn
Max Planck Institute for Polymer Research
347 PUBLICATIONS **7,587** CITATIONS
SEE PROFILE

Dmitry Turchinovich
Max Planck Institute for Polymer Research
89 PUBLICATIONS **591** CITATIONS
SEE PROFILE

THE JOURNAL OF PHYSICAL CHEMISTRY Letters

Letter

pubs.acs.org/JPCL

Ultrafast Terahertz Photoconductivity of Photovoltaic Polymer–Fullerene Blends: A Comparative Study Correlated with Photovoltaic Device Performance

Zuanming Jin,[†] Dominik Gehrig,[†] Clare Dyer-Smith,[†] Edwin J. Heilweil,[‡] Frédéric Laquai,[†] Mischa Bonn,[†] and Dmitry Turchinovich*,[†]

[†]Max Planck Institute for Polymer Research, Ackermannweg 10, 55128 Mainz, Germany

[‡]NIST - National Institute of Standards and Technology, 100 Bureau Drive, Gaithersburg, Maryland 20899, United States

ABSTRACT: Ultrafast photoinduced carrier dynamics in prototypical low band gap polymer:fullerene photovoltaic blend films PTB7:$PC_{70}BM$ and P3HT:$PC_{70}BM$ is investigated using ultrafast terahertz (THz) spectroscopy. The subpicosecond and few-picosecond decays of THz-probed photoconductivities for both compounds are observed, attributed to the rapid formation of polaron pairs by exciton–exciton annihilation and subsequent polaron pair annihilation, respectively. The transient THz photoconductivity spectra of PTB7:$PC_{70}BM$ are well described by the Drude–Smith (DS) model, directly yielding the important charge transport parameters such as charge carrier density, momentum scattering time, and effective localization. By comparison with P3HT:$PC_{70}BM$, we find that in PTB7:$PC_{70}BM$ the mobile charge carrier photoconductivity is significantly enhanced by a factor of 1.8 and prevails for longer times after charge formation, due to both improved mobile charge carrier yield and lower charge localization. In PTB7:$PC_{70}BM$, a strong dependency of electron momentum scattering time on electron density was found, well parametrized by the empirical Caughey–Thomas model. The difference in ultrafast photoconductivities of both P3HT:$PC_{70}BM$ and PTB7:$PC_{70}BM$ is found to correlate very well with the performance of photovoltaic devices based on those materials.

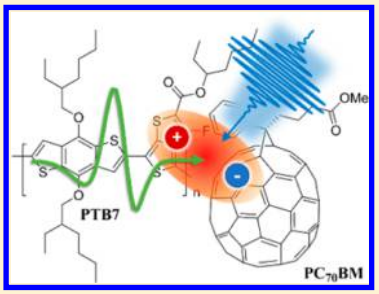

SECTION: Energy Conversion and Storage; Energy and Charge Transport

Bulk heterojunction (BHJ) organic solar cells have been investigated for over a decade and efficiencies in excess of 9% have now been realized.[1,2] Recently, Yu et al. have developed a series of novel donor polymers based on alternation of ester-substitued thieno [3,4-*b*] thiophene and benzodithiophene units (PTBX).[3,4] These low band gap polymers offer higher power conversion efficiency (PCE), owing to more effective solar photon harvesting in the region of the near-IR.[5] [6,6]-Phenyl-C61-butyric acid methyl ester (PCBM) has been demonstrated to be well intercalated into the PTBX polymer, and the reported PCE of PTB7/$PC_{70}BM$ exceeds 8%.[6]

A comprehensive understanding of charge generation, recombination, and transport in the BHJ is indispensable for optimizing new material systems. Ultrafast optical spectroscopic techniques provide details of the nonequilibrium carrier dynamics in organic photovoltaics; however, these studies cannot be directly correlated to the carrier mobilities.[7−9] Time-resolved terahertz spectroscopy (TRTS) on the other hand allows one to observe a subpicosecond (sub-ps)-resolved high-frequency photoconductive response of the material, yielding the ultrafast dynamics of photoinduced conductivity.[10−12] Moreover, in TRTS the nature of photoconductivity can be established by monitoring the real and imaginary components of the complex-valued terahertz (THz) conductivity spectrum, and the contributions from free and bound charges can be distinguished.[13−21] In contrast to the bulk mobility measured over micrometer-scale distances in devices for instance by the time-of-flight (TOF) technique,[22] TRTS can be used to extract the intrinsic mobility of carriers in the material in a noncontact way, free from the influence of extrinsic factors, such as applied fields and effects due to the interface between the electrode and the material. Furthermore, recent theoretical predictions by McGehee and co-workers have shown that the local mobility obtained by TRTS is a very valuable input parameter for kinetic Monte Carlo simulations of charge carrier separation at the donor–acceptor interface.[23] In fact, the simulations indicated that charge separation is facilitated by a high local charge carrier mobility—as can be measured by TRTS—because a high local charge carrier mobility increases the attempt frequency with which carriers try to undergo a separation process, in turn increasing the yield of spatially separated (free) charge carriers. Therefore, conductivity measurements by TRTS are an important source of information to reveal the fundamental mechanism of charge separation in bulk heterojunction organic solar cells.

In this Letter, we examine the dynamics of photoconductivity of photovoltaic PTB7:$PC_{70}BM$ blend on ultrafast, sub- and few-

Received: September 5, 2014
Accepted: October 10, 2014

   dx.doi.org/10.1021/jz501890n | *J. Phys. Chem. Lett.* 2014, 5, 3662−3668

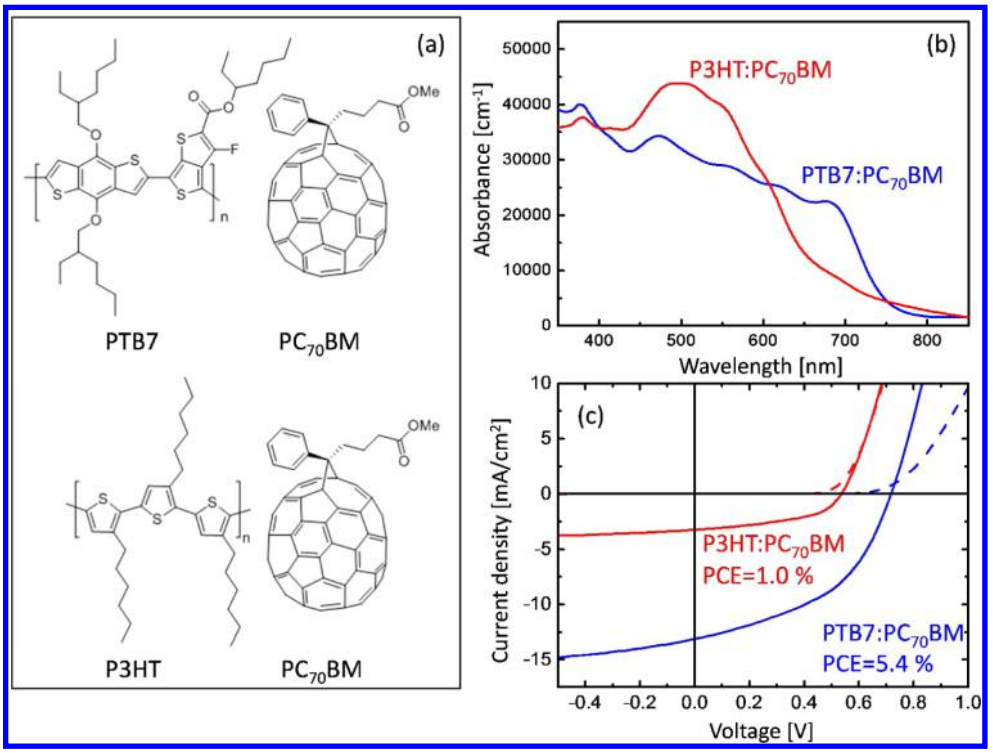

Figure 1. Characterization of the polymer−fullerene samples. (a) Chemical structures, (b) absorbance spectra, and (c) density−voltage (J−V) characteristics of PTB7:$PC_{70}BM$ and P3HT:$PC_{70}BM$ under AM1.5G-like conditions at 0.7 suns illumination conditions (solid lines) and dark conditions (dashed lines).

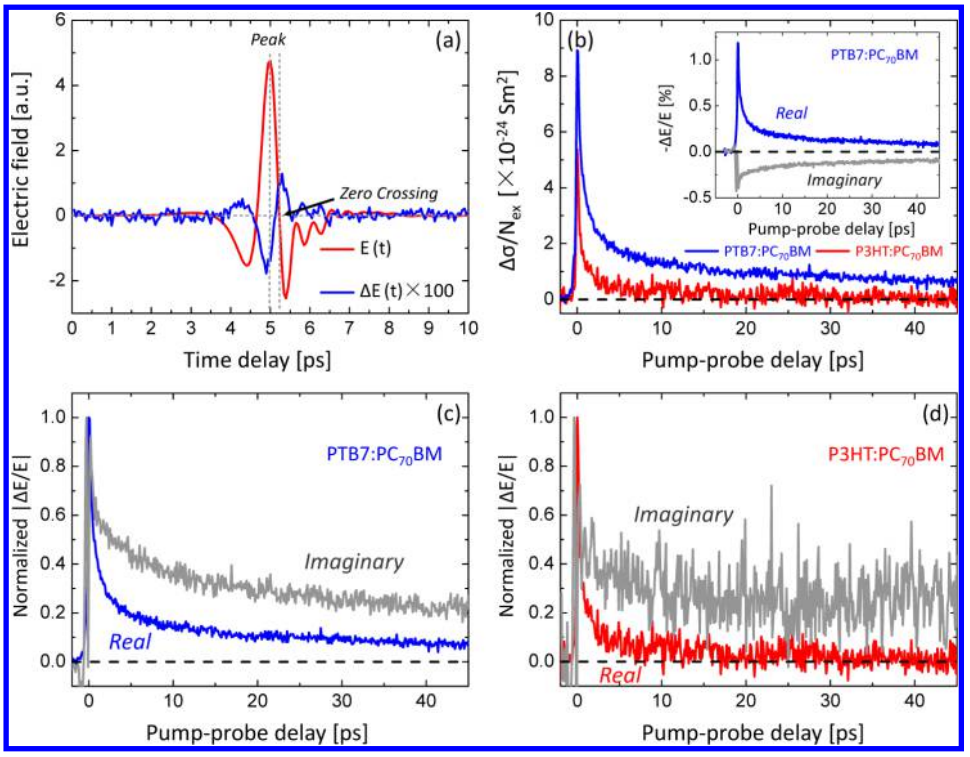

Figure 2. (a) The transmitted THz electric-field $E(t)$ and the photomodulation of the THz waveform $\Delta E(t, \Delta t = 2$ ps) in PTB7:$PC_{70}BM$ film. (b) Transient sheet real conductivity dynamics (frequency averaged conductivity) of PTB7:$PC_{70}BM$ and P3HT:$PC_{70}BM$ blend films, excited by 400 nm pulses with a sheet excitation density of $N_{ex} = 1.02 \times 10^{19}$ absorbed photons/m^2 for PTB7:$PC_{70}BM$ and of 0.5×10^{19} absorbed photons/m^2 for P3HT:$PC_{70}BM$, respectively. The THz real conductivity is scaled to the excitation density, N_{ex}. Inset: Pump−probe scans are performed at the peak and zero-crossing of the THz waveform, corresponding to the real and imaginary part of the photoconductivity of PTB7:$PC_{70}BM$. (c,d) The normalized real and imaginary photoconductivities for PTB7:$PC_{70}BM$ and P3HT:$PC_{70}BM$, respectively.

dx.doi.org/10.1021/jz501890n | J. Phys. Chem. Lett. 2014, 5, 3662−3668

ps time scales, and compare it with that of the archetypal P3HT:$PC_{70}BM$ system. Further, the PCE of photovoltaic devices based on both PTB7:$PC_{70}BM$ and P3HT:$PC_{70}BM$ blends is investigated, and is directly correlated with the ultrafast charge dynamics within the constituting materials. We find that the photoconductivity in the PTB7:$PC_{70}BM$ is significantly, by a factor of 1.8, enhanced, and that it is also about 3 times longer-lived than in the P3HT:$PC_{70}BM$ system under the same excitation conditions. A model describing the conduction of mobile charge carriers under long-range localization condition (Drude−Smith model, DS) reproduces our results very well, which allows one to factorize the measured ultrafast photoconductivity response into the carrier density, carrier momentum relaxation time, and the effective localization. The product of the quantum yields of excitation and carrier mobility, as well as the localization parameter c and the electron momentum scattering time of PTB7:$PC_{70}BM$ are compared to that of recently reported values for P3HT:PCBM. These observations demonstrate higher yield of mobile charge of PTB7:$PC_{70}BM$ as compared to that of P3HT:PCBM, beyond what is expected from the simple increase in total light harvesting capability.

Figure 1a,b shows the chemical structures of the donor and acceptor molecules involved, and typical steady state absorption spectra for PTB7:$PC_{70}BM$ and P3HT:$PC_{70}BM$ blend films, respectively. The absorption maxima of the PTB7:$PC_{70}BM$ and P3HT:$PC_{70}BM$ blends are at around 680 and 580 nm, respectively. The film thickness of PTB7:$PC_{70}BM$ was about 400 nm with optical density (OD) around 1.43, and the P3HT:$PC_{70}BM$ film thickness was about 65 nm with OD ∼ 0.27. Both ODs correspond to the optical wavelength of 400 nm. The layer thickness was determined with a Tencor P10 surface profilometer.

First, we present the performance of photovoltaic devices based on PTB7:$PC_{70}BM$ and P3HT:$PC_{70}BM$. As shown in the current density−voltage (J−V) curves in Figure 1c, the two blends clearly differ in their performance: PTB7:$PC_{70}BM$ (PCE = 5.41%) outperformed P3HT:$PC_{70}BM$ (PCE = 1.02%) by as much as a factor of 5. The strongest effect was in the measured short-circuit current density (J_{SC} = 12.60 mA/cm^2 for PTB7:$PC_{70}BM$ and 3.13 mA/cm^2 for P3HT:$PC_{70}BM$). Taking the different absorption properties into account, we can calculate the theoretical maximum for J_{SC} with a transfer matrix approach.[24] J_{SC} = 8.69 mA/cm^2 and 14.33 mA/cm^2 for P3HT:$PC_{70}BM$ and PTB7:$PC_{70}BM$, respectively, are expected under the assumption of an internal quantum efficiency (IQE) of unity and considering interference effects with an illumination intensity equal to 0.7 suns. Hence, in our case, the realized J_{SC} corresponds to 36% and 89% of the maximum value for P3HT:$PC_{70}BM$ and PTB7:$PC_{70}BM$, respectively, in agreement with the known variation in IQE in these systems.[24]

Now we proceed to describe the ultrafast THz measurements and their interpretations. In our measurements, the films of polymer blends were deposited on fused silica substrates, and the standard optical pump−THz probe measurements were carried out in transmission configuration.[10] All the measurements were carried out at room temperature and in dry nitrogen environment, to prevent the THz absorption by atmospheric water. Both blends under investigation were photoexcited at 400 nm wavelength corresponding to 3.1 eV photon energy, which is above the absorption gaps of both the donor and acceptor. A typical measurement of a single-cycle THz pulse transmitted through the PTB7:$PC_{70}BM$ film, $E(t)$ is shown as the red curve in Figure 2a. The pump-induced modulation of the THz field transmission is recorded as $\Delta E(t, \Delta t) = E_{pump}(t, \Delta t) - E(t)$. A typical ΔE (t, Δt = 2 ps) using 400 nm optical excitation, scaled by a factor of 100, is plotted as the blue curve in Figure 2a.

The change in peak amplitude of the THz waveform is proportional to the real part of the photoinduced conductivity, mostly arising from the influence of mobile charge carriers. The photoinduced phase shift of the THz waveform is in turn proportional to the imaginary part of the photoinduced conductivity, which can also contain contributions from polarization effects of bound charges, such as excitons.[21,25] The pump-induced phase-shift of the transmitted THz waveform to later times is indicative of pump-induced increase in the material polarizability, i.e., in the increase of its real-valued refractive index (which corresponds to a larger negative imaginary conductivity).[26] By varying the time delay between the 400 nm optical pump and THz probe pulses, we acquired the dynamics of the real (blue curve) and imaginary (gray curve) conductivity by measuring the photoinduced peak absorption and time-shift of the THz waveform, respectively, as shown in the inset of Figure 2b.

We first studied the sheet photoconductivity $\Delta\sigma_{2D}$, which can be reconstructed from the photoinduced peak change in the THz electric-field amplitude as a function of pump−probe time delay:[27,28]

$$\sigma_{2D} = \frac{1+n}{Z_0}\left(\frac{1}{1+\Delta E/E} - 1\right) \quad (1)$$

where n = 1.95 is the THz refractive index of the fused silica substrate, and Z_0 = 377 Ω is the impedance of free space. Figure 2b shows the pump-induced sheet real-valued conductivity $\Delta\sigma_{2D}$ scaled to the absorbed photon flux (with the flux being equal to excited electron density N_{ex}) as a function of pump−probe delay. In this case, the 400 nm optical excitation at a fluence of 530 μJ/cm^2 corresponded to the excited sheet densities of N_{ex} = 1.02 × 10^{19} and 0.5 × 10^{19} photons/m^2 for PTB7:$PC_{70}BM$ and P3HT:$PC_{70}BM$, respectively. We note here that the control measurements on neat PCBM were also performed, revealing both very low optical density at the excitation wavelength and the negligible photoconductivity of this material. The real-valued conductivity dynamics for both PTB7:$PC_{70}BM$ and P3HT:$PC_{70}BM$ exhibit a rise right after excitation within the instrumental time resolution (∼100 fs). Subsequently, a fast (<1 ps) decay is followed by a few-ps exponential decay, and then by a much slower (tens of ps) process. Comparing the scaled real-valued conductivity dynamics of these two blend polymers (Figure 2b), we find an enhancement of the photoconductivity scaled to the sheet density upon replacing the P3HT donor with the low band gap polymer PTB7 by a factor of ∼1.8, indicative of the enhanced generation of mobile charge carriers (i.e., the product of the quantum yield and mobility) in the latter blend. Moreover, the real-valued photoconductivity remains nonzero in PTB7:$PC_{70}BM$ at delay times exceeding 40 ps, indicating the persistence of mobile charge carriers over much longer times than in the P3HT:$PC_{70}BM$ blend, where the mobile carriers live only for about 10 ps. On the other hand, as shown by the normalized absolute value of $|\Delta E/E(t)|$ for the THz amplitude attenuation and the phase shift for two blends in Figure 2c,d, the imaginary conductivity decays much more slowly than the real one for both blends. This means that the polarization-

dx.doi.org/10.1021/jz501890n | J. Phys. Chem. Lett. 2014, 5, 3662−3668

dominated component of THz response, and hence the photoinduced *bound* electron−hole pairs live significantly longer than the mobile charge carriers in both compounds. We, however, cannot make any definite statements about the nature of these bound charge carriers. In P3HT:$PC_{70}BM$, a negative imaginary conductivity and a nearly zero real conductivity were found after 20 ps, i.e., only the bound charges are found in P3HT:$PC_{70}BM$ at delay times exceeding 20 ps.[17]

Figure 3a compares the peak-normalized evolution of the photoconductivity with triexponential fits, which reveals the

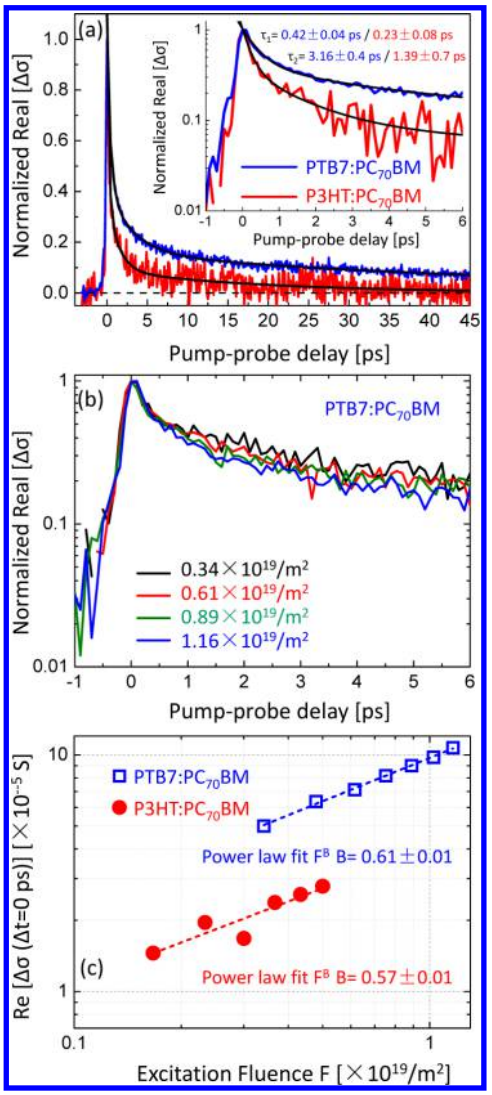

Figure 3. (a) The transient real conductivity dynamics of two blend films normalized to unity. Lines are triexponential fits (see text). Inset initial conductivity dynamics in the two blend films. (b) Normalized transient THz real conductivities of PTB7:$PC_{70}BM$ with increased excitation fluence, from top to bottom. (c) Excitation fluence dependence of the real photoconductivity taken at zero-delay time for PTB7:$PC_{70}BM$ (blue squares) and P3HT:$PC_{70}BM$ (red circles). The dashed lines are power-law fits to the data.

difference between these two BHJ blends. For the P3HT:$PC_{70}BM$, the photoconductivity drops by ca. 65% within $\tau_1 = 0.23 \pm 0.08$ ps and then 27% within $\tau_2 = 1.39 \pm 0.7$ ps, in contrast to a much slower decay in PTB7:$PC_{70}BM$: 62% within $\tau_1 = 0.42 \pm 0.04$ ps and then a further 23% within $\tau_2 = 3.16 \pm 0.4$ ps. In Figure 3b, the normalized time-resolved THz photoconductivity in PTB7:$PC_{70}BM$ is shown, and the initial sub-ps process is almost independent of excitation density, while the few-ps decay process becomes slightly faster upon increasing the photoexcitation fluence. Figure 3c shows the peak magnitude of real-valued photoconductivity as a function of excitation fluence for two blends in double-logarithmic representation. We find the best fits by a power law of the form: $\Delta\sigma_{peak} = AF^B$,[29] with $B = 0.61 \pm 0.01$ and 0.57 ± 0.01 for PTB7:$PC_{70}BM$ and P3HT:$PC_{70}BM$, respectively. This observed sublinear fluence dependence of the initial photoresponse can be explained by initial charge generation followed by exciton−exciton annihilation.[30] Therefore, the instantaneous rise of the real conductivity at time zero can be attributed to the exciton−exciton annihilation upon photoexcitation. After exciton splitting, charge transfer (CT) states or polaron pairs are formed at the donor−acceptor interface on the sub-ps time scale, in which the charges still attract each other Coulombically.[2,3,31,32] As the distance between photogenerated polaron pairs becomes smaller at high excitation densities, little charge diffusion is required for electron−hole recombination, which could explain the fact that the observed few-ps decay becomes increasingly faster as the excitation fluence increases from 0.34×10^{19} m^{-2} to 1.16×10^{19} m^{-2}. The several-ps decay therefore is best assigned to polaron pair annihilation.[31] The slow time dynamics occur on the time scale of 56 ± 5 ps and 20 ± 5 ps for PTB7:$PC_{70}BM$ and P3HT:$PC_{70}BM$, respectively, which arises from carrier cooling and trapping in the blends.

The big advantage of the TRTS measurement is in the ability to determine the complex-valued, THz frequency-resolved photonconductivity spectrum of the material under study at various delay times, Δt. Both the real and imaginary parts of the frequency-dependent photoconductivity $\Delta\sigma(\omega, \Delta t)$ are derived from $E(t)$ and $\Delta E(t, \Delta t)$ through Fourier transform without having to resort to the Kramers−Kronig relations.[10] Figure 4 shows the photoconductivity spectra of a PTB7:$PC_{70}BM$ blend film with photoexcitation density of 1.02×10^{19} m^{-2} at five representative time delays. The shape of the photoconductivity spectrum changes slightly with increasing time delay. The nonzero value of the real conductivity evident in the data at low frequency suggests that the response in PTB7:$PC_{70}BM$ is dominated by the mobile charge carriers. Similar to previous reports for P3HT:PCBM,[14] the imaginary part is negative and decreases with increasing frequency approaching zero at the lowest frequency. In disordered media, the conductivity spectra can often be well-described by the model of mobile charge conduction under the condition of long-range localization—the DS model:[33−36]

$$\tilde{\sigma}_{DS}(\omega) = \frac{\varepsilon_0 \omega_p^2 \tau}{1 - i\omega\tau}\left(1 + \frac{c}{1 - i\omega\tau}\right) \quad (2)$$

where ε_0 is the vacuum permittivity, ω_p is the plasma frequency, and τ is the momentum relaxation time. The localization degree parameter c denotes the probability that a carrier maintains its velocity during scattering (between −1 and 0). $c = 0$ implies full momentum randomized scattering (and hence eq 2 is reduced to a classical Drude formula),[26] while negative c indicates that the carrier undergoes preferential backscattering, i.e. localization, for example, when reaching the edge of a local potential well. Equation 2 is used to fit the measured real and imaginary parts of $\tilde{\sigma}(\omega)$ with very good agreement between the data and the model, yielding the τ, ω_p, and c. Charge mobility depends

dx.doi.org/10.1021/jz501890n | J. Phys. Chem. Lett. 2014, 5, 3662−3668

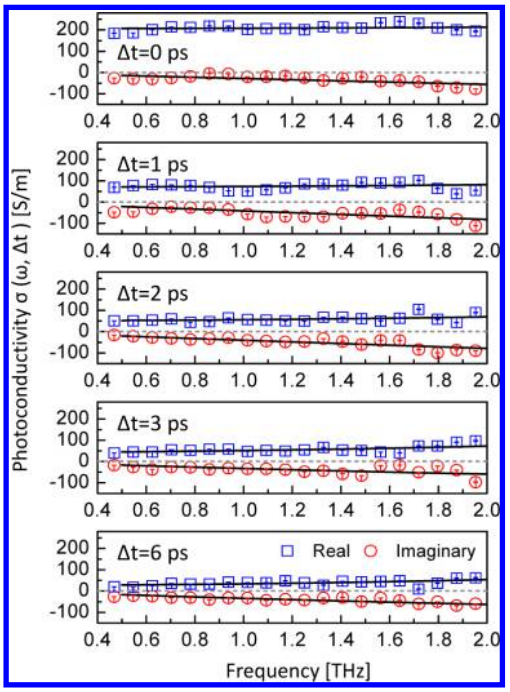

Figure 4. Frequency dependence of the real (blue squares) and imaginary (red circles) photoconductivity in PTB7:$PC_{70}BM$, measured at Δt = 0, 1, 2, 3, and 6 ps after photoexcitation. The solid lines are fits to the DS model described in the text.

on two quantities, effective mass m^* and scattering time τ, through the relation $\mu = e\tau/m^*$, where e is the elementary charge.[37] The density of excited carriers N is related to the plasma frequency $N = (\varepsilon_0\omega_p^2 m^*/e^2)$ and then the DC conductivity is given by $\sigma_{DC} = eN\mu(1 + c)$. Effective mass $m^* = 1.7m_e$ is assumed to be the same as in P3HT.

In our experiments we were only able to measure the frequency-resolved THz conductivity spectra for PTB7:$PC_{70}BM$ blend, while the much weaker and shorter-lived photoconductive response of P3HT:$PC_{70}BM$ did not allow for frequency-resolved spectroscopy within the signal-to-noise ratio of our spectrometer. However, we are able to relate our findings on PTB7:$PC_{70}BM$ (Figure 4) with the results of the similar experiment by Cunningham et al. on P3HT:PCBM (ref 14), also showing a clear DS conductivity response. Figure 5 summarizes the results of the DS model fit to the frequency-dependent complex conductivity of PTB7:$PC_{70}BM$ (this work, blue circles) and the P3HT:PCBM 1:1 blend with 400 nm excitation from ref 14 (red squares). The DC conductivity σ_{DC} normalized by the excited charge density eN_{ex}, which corresponds to the product of the quantum yields of excitation $\eta = N/N_{ex}$ and the DC mobility μ_{DC}, $\eta \times \mu_{DC}$, an intrinsic material response, drops significantly during the first ps and is larger for PTB7:$PC_{70}BM$ than that for P3HT: $PC_{70}BM$, as shown in Figure 5a.

In Figure 5b, the localization parameter $-c$ is shown. As mentioned above, the polaron pair formation on a sub-ps time scale acts as a potential well that hinders the movement of mobile charge, which is seen here as a rapid decrease in $\eta \times \mu_{DC}$, and in localization parameter c approaching -1. Comparing the average value and the rate of increase of with pump−probe delay of the parameter $-c$ for two blends, we note that PTB7:$PC_{70}BM$ is consistently smaller ($\langle -\bar{c} \rangle = 0.91 \pm 0.04$ and 0.97 ± 0.02 for PTB7:$PC_{70}BM$ and P3HT:$PC_{70}BM$,

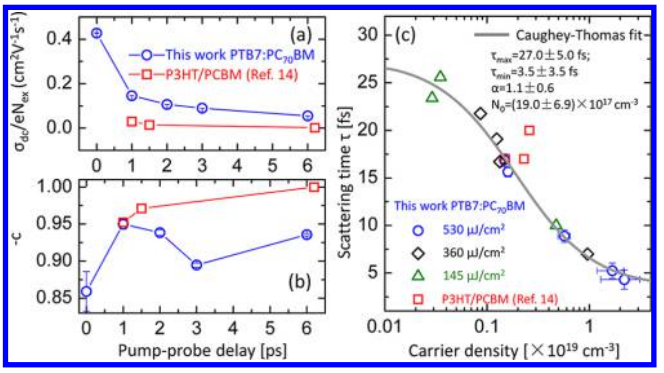

Figure 5. Results of DS model fit to the frequency dependent complex conductivity of PTB7:$PC_{70}BM$ in current work (blue circles) and the results of P3HT:PCBM 1:1 blend with 400 nm excitation from ref 14 (red squares). (a) DC photoconductivity σ_{DC} normalized by the excited carrier density eN_{ex} and (b) Parameter -c as a function of pump−probe delay time. (c) Carrier density dependence of the electron momentum scattering time τ. The circles, triangles and rhombus correspond to the data obtained at various pump fluences, for varying delay times. Solid line shows the Caughey−Thomas fit with parameters.

respectively) and has a lower rate of increase, indicating more efficient separation of electrons and holes in PTB7:$PC_{70}BM$ than in P3HT:$PC_{70}BM$.

With knowledge of the carrier densities $N(\Delta t)$ for each pump−probe delay, we are now able to correlate the electron momentum scattering time τ with the corresponding values of carrier densities $N(\Delta t)$, as shown in Figure 5c. In the carrier density range presented here, τ decreases drastically from ∼26 fs down to ∼4 fs, as the carrier density increases by about 2 orders of magnitude in a range of 3×10^{23} to 223×10^{23} m^{-3}. This decrease in electron scattering time in polymer blends with increasing carrier density could be explained by the carrier−carrier scattering, rather than the enhanced electron−phonon and electron−defect interactions caused by phase-space filling as is typical for crystalline semiconductors, such as GaAs,[38] and TiO_2.[39] We have found that the measured dependency of electron momentum relaxation time on electron density $\tau(N)$ can be very well parametrized by an empirical Caughey−Thomas relation traditionally used for crystalline semiconductors,[40] $\tau = ((\tau_{max} - \tau_{min})/(1 + (N/N_0)^{\alpha})) + \tau_{min}$, where $\tau_{max,min}$, N_0 and α are the fit parameters. Best fit parameters are shown in Figure 5c. We note that for the low excitation conditions under normal solar irradiance, τ_{max} = 27 fs is the relevant material parameter.

In summary, we have studied the transient THz conductivity of the low band gap polymers PTB7 and P3HT blended with the electron acceptor $PC_{70}BM$ using ultrafast THz spectroscopy. Compared to P3HT:$PC_{70}BM$, $\eta \times \mu_{DC}$, the quantum efficiency for charge generation multiplied by the carrier mobility, is enhanced significantly, by a factor of 1.8 in PTB7:$PC_{70}BM$. The mobile-charge photoconductivity persists over longer delays over 60 ps in PTB7:$PC_{70}BM$, while in P3HT:$PC_{70}BM$ it decays quickly within about 20 ps leaving only the signatures of photoinduced polarization by bound electron−hole pairs. The enhanced formation of polaron pairs and looser localization correspond well with the improved internal quantum efficiency, and ultimately with higher photovoltaic device performance in PTB7:$PC_{70}BM$ blends as compared to P3HT:$PC_{70}BM$, measured in this work. Yet, other factors, e.g., related to both the photoexcitation density and

dx.doi.org/10.1021/jz501890n | J. Phys. Chem. Lett. 2014, 5, 3662−3668

photovoltaic device manufacturing might contribute as well. Finally, our results demonstrate that carrier−carrier interaction at higher density is playing a significant role in decreasing the charge carrier mobility in PTB7:$PC_{70}BM$.

EXPERIMENTAL METHODS

Photovoltaic Device Preparation. For the preparation of solar cells, indium tin oxide (ITO)-coated glass substrates (Präzisions Glas & Optik GmbH, Germany) were patterned by wet etching and cleaned by successive ultrasonication in detergent, acetone, then *iso*-propanol. Subsequently, the samples were treated with an argon plasma for 15 min prior to spin-coating of a ∼ 40 nm poly(3,4-ethylene-dioxythiophene): poly(styrenesulfonate) (PEDOT:PSS) (Clevios P VP Al 4083, H. C. Stark) layer. The substrates were transferred into a nitrogen-filled glovebox and heated to 120 °C for 30 min. For the active layer deposition, PTB7 (1-Material, M_w = 210 000, PDI = 4.1) and $PC_{70}BM$ (Solenne BV) were dissolved separately in chlorobenzene with 3 vol % 1,8-diiodooctane (DIO) at a concentration of 25 mg mL^{-1}. P3HT (BASF Sepiolid P200, Mw =20899.6, PDI = 1.75) and $PC_{70}BM$ were dissolved separately in 1,2-dichlorobenze (o-DCB) at a concentration of 25 mg mL^{-1}. The solutions were stirred overnight at 70 °C. Four hours before spin-coating the active layer the solutions were mixed in a donor:acceptor ratio of 1:1.5 (by weight), and the blends were then spin-coated at 900 rpm for 60 s, resulting in an active layer thickness of ∼400 nm for PTB7:$PC_{70}BM$ and ∼65 nm for P3HT:$PC_{70}BM$ films. As a top-electrode, a bilayer of 5 nm calcium and 100 nm aluminum was evaporated through a shadow mask. THz spectroscopic samples were fabricated in the same way except that fused silica substrates were used and no top-electrode was evaporated. Solar cells were characterized with a solar simulator (K. H. Steuernagel Lichttechnik GmbH, Germany) employing a 575 W metal halide lamp combined with a filter system to create a spectrum according to AM1.5G conditions, however, with a lower intensity of 70 mW cm^{-2}. Current−voltage curves were taken with a Keithley 236 Source Measure Unit (SMU) in a glovebox.

Terahertz Spectroscopy. Our THz setup was driven by Ti:sapphire femtosecond amplifier, operating at repetition rate of 1 kHz, and generating 120 fs pulses at central wavelength 800 nm. A part of the laser output was used as a pump pulse, after second harmonics with a b-BaB_2O_4 (BBO) crystal for above the band gap of the PTB7:$PC_{70}BM$ excitation at 400 nm, with the pump fluence of 530 $\mu J/cm^2$. Another part was used to generate and detect the THz radiation by optical rectification and electro-optical sampling with ZnTe nonlinear crystals. Both optical pump and THz probe pulses were incident on the sample at normal incidence. The in-plane conductivity of the photoexcited sample was probed with the THz pulse. Time-resolved data were obtained by averaging 5 time-delay scans. The TRTS measurement enclosure was purged with N_2 to minimize photo-oxidization and water vapor interference effects. No significant degradation was observed during the experiments. All measurements were performed at room-temperature.

AUTHOR INFORMATION

Corresponding Author

*E-mail: turchino@mpip-mainz.mpg.de.

Notes

The authors declare no competing financial interest.

ACKNOWLEDGMENTS

D.T. acknowledges EU Career Integration Grant 334324 LIGHTER, and the Max Planck Society for financial support. F.L. thanks the Max Planck Society for funding the Max Planck Research Group of Organic Optoelectronics and the Deutsche Forschungsgemeinschaft (DFG) for funding in the framework of the priority program SPP1355 "Elementary Processes in Organic Phtovoltaics". D. G. acknowledges a Kekulé scholarship of the Fonds der Chemischen Industrie (FCI).

REFERENCES

(1) Brabec, C. J.; Gowrisanker, S.; Halls, J. J. M.; Laird, D.; Jia, S.; Williams, S. P. Polymer−Fullerene Bulk-Heterojunction Solar Cells. *Adv. Mater.* **2010**, *22*, 3839−3856.

(2) Clarke, T. M.; Durrant, J. R. Charge Photogeneration in Organic Solar Cells. *Chem. Rev.* **2010**, *110*, 6736−6767.

(3) Szarko, J. M.; Rolczynski, B. S.; Lou, S. J.; Xu, T.; Strzalka, J.; Marks, T. J.; Yu, L.; Chen, L. X. Photovoltaic Function and Exciton/Charge Transfer Dynamics in a Highly Efficient Semiconducting Copolymer. *Adv. Funct. Mater.* **2014**, *24*, 10−26.

(4) Liang, Y.; Wu, Y.; Feng, D.; Tsai, S.-T.; Son, H.-J.; Li, G.; Yu, L. Development of New Semiconducting Polymers for High Performance Solar Cells. *J. Am. Chem. Soc.* **2009**, *131*, 56−57.

(5) Liu, F.; Zhao, W.; Tumbleston, J. R.; Wang, C.; Gu, Y.; Wang, D.; Briseno, A. L.; Ade, H.; Russell, T. P. Understanding the Morphology of PTB7:PCBM Blends in Organic Photovoltaics. *Adv. Energy Mater.* **2014**, *4*, 1301377.

(6) Chen, H.-Y.; Hou, J.; Zhang, S.; Liang, Y.; Yang, G.; Yang, Y.; Yu, L.; Wu, Y.; Li, G. Polymer Solar Cells with Enhanced Open-Circuit Voltage and Efficiency. *Nat. Photonics* **2009**, *3*, 649−653.

(7) Dimitrov, S. D.; Bakulin, A. A.; Nielsen, C. B.; Schroeder, B. C.; Du, J.; Bronstein, H.; McCulloch, I.; Friend, R. H.; Durrant, J. R. On the Energetic Dependence of Charge Separation in Low-Band-Gap Polymer/Fullerene Blends. *J. Am. Chem. Soc.* **2012**, *134*, 18189−18192.

(8) Yonezawa, K.; Kamioka, H.; Yasuda, T.; Han, L.; Moritomo, Y. Fast Carrier Formation from Acceptor Exciton in Low-Gap Organic Photovotalic. *Appl. Phys. Express* **2012**, *5*, 042302.

(9) Howard, I. A.; Mauer, R.; Meister, M.; Laquai, F. Effect of Morphology on Ultrafast Free Carrier Generation in Polythiophene:-Fullerene Organic Solar Cells. *J. Am. Chem. Soc.* **2010**, *132*, 14866−14876.

(10) Ulbricht, R.; Hendry, E.; Shan, J.; Heinz, T. F.; Bonn, M. Carrier Dynamics in Semiconductors Studied with Time-Resolved Terahertz Spectroscopy. *Rev. Mod. Phys.* **2011**, *83*, 543−586.

(11) Tonouchi, M. Cutting-Edge Terahertz Technology. *Nat. Photonics* **2007**, *1*, 97−105.

(12) Baxter, J. B.; Guglietta, G. W. Terahertz Spectroscopy. *Anal. Chem.* **2011**, *83*, 4342−4368.

(13) Esenturk, O.; Melinger, J. S.; Heilweil, E. J. Terahertz Mobility Measurements on Poly-3-hexylthiophene Films: Device Comparison, Molecular Weight, and Film Processing Effects. *J. Appl. Phys.* **2008**, *103*, 023102.

(14) Cunningham, P. D.; Hayden, L. M. Carrier Dynamics Resulting from Above and Below Gap Excitation of P3HT and P3HT/PCBM Investigated by Optical-Pump Terahertz-Probe Spectroscopy. *J. Phys. Chem. C* **2008**, *112*, 7928−7935.

(15) Esenturk, O.; Kline, R. J.; Delongchamp, D. M.; Heilweil, E. J. Conjugation Effects on Carrier Mobilities of Polythiophenes Probed by Time-Resolved Terahertz Spectroscopy. *J. Phys. Chem. C* **2008**, *112*, 10587−10590.

(16) Němec, H.; Nienhuys, H.-K.; Zhang, F.; Inganas, O.; Yartsev, A.; Sundstrom, V. Charge Carrier Dynamics in Alternating Polyfluorene

Copolymer: Fullerene Blends Probed by Terahertz Spectroscopy. *J. Phys. Chem. C* **2008**, *112*, 6558−6563.
(17) Ai, X.; Beard, M. C.; Knutsen, K. P.; Shaheen, S. E.; Rumbles, G.; Ellingson, R. J. Photoinduced Charge Carrier Generation in a Poly(3-hexylthiophene) and Methanofullerene Bulk Heterojunction Investigated by Time-Resolved Terahertz Spectroscopy. *J. Phys. Chem. B* **2006**, *110*, 25462−25471.
(18) Hendry, E.; Schins, J. M.; Candeias, L. P.; Siebbeles, L. D. A.; Bonn, M. Efficiency of Exciton and Charge Carrier Photogeneration in a Semiconducting Polymer. *Phys. Rev. Lett.* **2004**, *92*, 196601.
(19) Němec, H.; Nienhuys, H.-K.; Perzon, E.; Zhang, F. L.; Inganäs, O.; Kužel, P.; Sundström, V. Ultrafast Conductivity in a Low-Band-Gap Polyphenylene and Fullerene Blend Studied by Terahertz Spectroscopy. *Phys. Rev. B* **2009**, *79*, 245326.
(20) Ponseca, C. S., Jr.; Němec, H.; Vukmirovi, N.; Fusco, S.; Wang, E.; Andersson, M. R.; Chabera, P.; Yartsev, A.; Sundström, V. Electron and Hole Contributions to the Terahertz Photoconductivity of a Conjugated Polymer: Fullerene Blend Identified. *J. Phys. Chem. Lett.* **2012**, *3*, 2442−2446.
(21) Wang, F.; Shan, J.; Islam, M. A.; Herman, I. P.; Bonn, M.; Heinz, T. F. Exciton Polarizability in Semiconductor Nanocrystals. *Nat. Mater.* **2006**, *5*, 861−864.
(22) Mauer, R.; Kastler, M.; Laquai, F. The Impact of Polymer Regioregularity on Charge Transport and Efficiency of P3HT:PCBM Photovoltaic Devices. *Adv. Funct. Mater.* **2010**, *20*, 2085−2092.
(23) Burke, T. M.; McGehee, M. D. How High Local Charge Carrier Mobility and an Energy Cascade in a Three-Phase Bulk Heterojunction Enable >90% Quantum Efficiency. *Adv. Mater.* **2014**, *26*, 1923−1928.
(24) Burkhard, G. F.; Hoke, E. T.; McGehee, M. D. Accounting for Interference, Scattering, and Electrode Absorption to Make Accurate Internal Quantum Efficiency Measurements in Organic and Other Thin Solar Cells. *Adv. Mater.* **2010**, *22*, 3293−3297.
(25) Jensen, S. A.; Ulbricht, R.; Narita, A.; Feng, X.; Müllen, K.; Hertel, T.; Turchinovich, D.; Bonn, M. Ultrafast Photoconductivity of Graphene Nanoribbons and Carbon Nanotubes. *Nano Lett.* **2013**, *13*, 5925−5930.
(26) Dressel, M.; Grüner, G. *Electrodynamics of Solids: Optical Properties of Electrons in Matter*; Cambridge University Press: Cambridge, U.K., 2002.
(27) Lui, K. P. H.; Hegmann, F. A. Ultrafast Carrier Relaxation in Radiation-Damaged Silicon on Sapphire Studied by Optical-Pump−Terahertz-Probe Experiments. *Appl. Phys. Lett.* **2001**, *78*, 3478−3480.
(28) Porte, H. P.; Jepsen, P. U.; Daghestani, N.; Rafailov, E. U.; Turchinovich, D. Ultrafast Release and Capture of Carriers in InGaAs/GaAs Quantum Dots Observed by Time-Resolved Terahertz Spectroscopy. *Appl. Phys. Lett.* **2009**, *94*, 262104.
(29) Parkinson, P.; Lloyd-Hughes, J.; Johnston, M. B.; Herz, L. M. Efficient Generation of Charges via Below-Gap Photoexcitation of Polymer-Fullerene Blend Films Investigated by Terahertz Spectroscopy. *Phys. Rev. B* **2008**, *78*, 115321.
(30) Dicker, G.; de Haas, M. P.; Siebbeles, L. D. A. Signature of Exciton Annihilation in the Photoconductance of Regioregular Poly(3-hexylthiophene). *Phys. Rev. B* **2005**, *71*, 155204.
(31) Ponseca, C. S., Jr.; Yartsev, A.; Wang, E.; Andersson, M. R.; Vithanage, D.; Sundström, V. Ultrafast Terahertz Photoconductivity of Bulk Heterojunction Materials Reveals High Carrier Mobility up to Nanosecond Time Scale. *J. Am. Chem. Soc.* **2012**, *134*, 11836−11839.
(32) Martini, I. B.; Smith, A. D.; Schwartz, B. J. Exciton-Exciton Annihilation and the Production of Interchain Species in Conjugated Polymer Films: Comparing the Ultrafast Stimulated Emission and Photoluminescence Dynamics of MEH-PPV. *Phys. Rev. B* **2004**, *69*, 035204.
(33) Anderson, P. W. Absence of Diffusion in Certain Random Lattices. *Phys. Rev.* **1958**, *109*, 1492−1505.
(34) Cooke, D. G.; Krebs, F. C.; Jepsen, P. U. Direct Observation of Sub-100 fs Mobile Charge Generation in a Polymer−Fullerene Film. *Phys. Rev. Lett.* **2012**, *108*, 056603.
(35) Smith, N. V. Classical Generalization of the Drude Formula for the Optical Conductivity. *Phys. Rev. B* **2001**, *64*, 155106.
(36) Unuma, T.; Yamada, N.; Nakamura, A.; Kishida, H.; Lee, S.-C.; Hong, E.-Y.; Lee, S.-H.; Kwon, O.-P. Direct Observation of Carrier Delocalization in Highly Conducting Polyaniline. *Appl. Phys. Lett.* **2013**, *103*, 053303.
(37) Cunningham, P. D.; Hayden, L. M.; Yip, H.-L.; Jen, A. K.-Y. Charge Carrier Dynamics in Metalated Polymers Investigated by Optical-Pump Terahertz-Probe Spectroscopy. *J. Phys. Chem. B* **2009**, *113*, 15427−15432.
(38) Mics, Z.; D'Angio, A.; Jensen, S. A.; Bonn, M.; Turchinovich, D. Density-Dependent Electron Scattering in Photoexcited GaAs in Strongly Diffusive Regime. *Appl. Phys. Lett.* **2013**, *102*, 231120.
(39) Hendry, E.; Koeberg, M.; Pijpers, J.; Bonn, M. Reduction of Carrier Mobility in Semiconductors Caused by Charge-Charge Interactions. *Phys. Rev. B* **2007**, *75*, 233202.
(40) Caughey, D. M.; Thomas, R. E. Carrier Mobilities in Silicon Empirically Related to Doping and Field. *Proc. IEEE* **1967**, *55*, 2192−2193.